Comparative study of solar cell technologies

Afonso Pedro Nunes da Silva Ravasco
afonso.ravasco@tecnico.ulisboa.pt

Instituto Superior Técnico, Universidade de Lisboa, Lisboa, Portugal

***Abstract*—When you think about sustainable energy, the first one that comes to mind is always solar power. It is amazing to think that photovoltaic (PV) technologies have been around for more than 70 years and it has evolved from just a small scientific research paper to a million dollar market. Throughout these whole 70 years, many materials have been subjected into tests and experiments, creating several photovoltaic generations. In this work, some of these generations will be compared with one another, in order to see what were the significant changes, not only in the material, but what do these materials contribute to for the photovoltaic community. To better study these materials, a 2D solar cell PIN model was developed using the software *COMSOL Multiphysics*. The designed model was produced with an electrical approach in mind, where its features such as the doping of the semiconductor and the incident wavelength can be user-defined. In addition, experimental tests were also adopted, in order to have real case scenario of the types of solar panels at hand as well as a SEM analysis of the same solar panels, to obtain a better understanding of the internal layers.**

I. Introduction

Solar technology has came a long way since the design of the first crystalline silicon solar cell back in 1954 in the Bell Laboratories, USA, registering an efficiency of about 4%. Nowadays, crystalline silicon solar cells are able to produce efficiencies above 25% and the continuous research of solar cells allowed the creation of thin-film solar cells and later the first solar cell made purely of organic materials, each of them marking different generations within the history of PV technology. [3] There are mainly two materials that are going to be subjected under analysis in this study: CIGS and silicon. Silicon representing the 1st generation of solar cells, is known for its market domination and be the lead material in solar panel production. It is known to produce very high efficiencies and have a wide absorption range. CIGS on the other hand is representing the 2nd generation, specifically the thin-film technology. Thin-films are known to use much less material than other solar cells and recently have achieved very high results. However, some of the CIGS cells contain toxic elements, like cadmium, which benefits their efficiency, but there are other types of CIGS that can be cadmium free. During this study, the creation of a 2D model of a solar cell was set to be the main goal. The model to be used was defined to be an approximation of an actual solar cell, mainly focused on the absorber layer, responsible for generating electron-hole pairs. This model was designed with the *COMSOL Multiphysics* software and originally the 2D model was based on a sample module of a Gallium Arsenide PIN photodiode which was later altered to fit the goal of the study. Lastly, real case scenarios will also be taken into consideration, in order to study the materials more extensively. To complement this experimental component, a SEM analysis will be used as well, mainly to determine the inside layers of the studied materials.

II. Target application

A. Electrical properties of a p-n junction

The p-n junction is commonly used for solar cells. This junction creates a charge separation of electron and holes and when the junction is formed, the large carrier concentration gradients cause the diffusion of carriers, i.e., holes diffuse from p-type semiconductors to n-type semiconductors and electrons diffuse from the way around. Because of the ionized impurity atoms, a layer without mobile charge carriers is formed when the electrons and holes diffuse across the junction, hence creating an electric field in this area which is called the depletion region. [2] [11].

Once the drift current is balanced by the diffusion the thermal equilibrium is established. At this point, the Fermi levels of the p-type semiconductor and n-type semiconductor are equal as it can be seen in Figure 1.

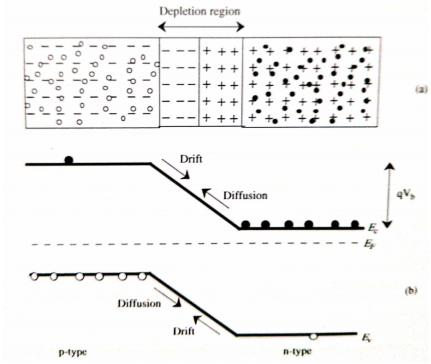

Fig. 1. a) Schematic structures of a p-n junction b) Its energy band diagram in thermal equilibrium. [11]

B. Equations used in the model

In this section, the equations that were used in the *COMSOL Multiphysics* model are going to be broken down. Since it was used two modules to design the solar cell, this section will divide into the semiconductor module, responsible for defining the material properties of the solar cell, and the electromagnetic waves module, responsible for generating the incident light onto the solar cell.

1) Semiconductor module: Firstly, the semiconductor material model is used and this model is the central node of the semiconductor module, since it defines the basic principles of the semiconductor. The main parameters of the semiconductor are defined in this section, such as the relative permittivity, the electron affinity, band gap and so on. The basic equations that operate in this region are the equations related to the definition of the conduction and valence bands (Equation 2 and 3 respectively), the current density of electrons and holes (Equations 4 and 5, respectively) and the semiconductor's charge density (Equation 1).

$$\rho = q(p - n + N_d^+ - N_a^-) \tag{1}$$

$$E_c = -(V + \chi_0) \tag{2}$$

$$E_v = -(V + \chi_0 + E_{g,0}) \tag{3}$$

$$J_n = qn\mu_n \nabla E_c + \mu_n k_B T G(n/N_c)\nabla n + qnD_n \nabla \ln(T) \tag{4}$$

$$J_p = qp\mu_p \nabla E_v + \mu_n k_B T G(p/N_v)\nabla p + qpD_p \nabla \ln(T) \tag{5}$$

Where, the k_B is the Boltzmann constant, G is the Generation rate. D_n and D_p are the drift diffusion coefficients of electron and hole respectively.

The next step to be considered in the model is the doping. There are two types of doping.

The analytic doping density allows the user to specify in a block-shaped region the doping to be defined, along with the decay profile away from the region, approximating it to a diffusion process. The decay of the dopant is defined by the specification of a junction depth, d_j, given by the following equations.

$$N_{A,D} = N_{A,D}^{user} \tag{6}$$

$$l_x = l_y = \frac{d_j}{\sqrt{\ln\left(\left|\frac{N_{A0}}{N_b}\right|\right)}} \tag{7}$$

If the region is n-doped, then the first index of the equation should be considered (acceptors), but if a p-doped region is preferred then the second index of the equations is used (donors).

This type of doping is the one used to define the p-doped layer and the n-doped layer, later in the model (Chapter 4).

On the other hand, there is also the geometric doping model, which works in parallel with the analytic model. This enables the doping profiles to be expressed as a function of distance from selected boundaries. The junction depth is applied here as well and it specifies the distance from the selected boundaries at which the dopant concentration is equal to the specified background doping. In other words, this doping model dopes the boundary of the semiconductor all the way until the junction depth, hence creating the p+ doping contact and the n+ doping contact in the model.

2) Electromagnetic Waves module: The Electromagnetic Waves module was also used in the model to recreate the incident radiation. The following equations represent how the electric field is calculated for every point in the domain (solar cell).

$$\nabla \times (\nabla \times \mathbf{E}) - k_0^2 \epsilon_r \mathbf{E} = \mathbf{0} \tag{8}$$

Given that, ϵ_r

$$\epsilon_r = (n - ik)^2 \tag{9}$$

Where, n and k are respectively, the real and imaginary part of the refractive index.

$$\mathbf{E}(x, y, z) = (x, y)e^{-ik_z z} \tag{10}$$

Where, k_z is the wave's propagation constant.

III. PV TECHNOLOGY TREE

The Solar cell technology has been evolving over the last 50 years. There have been many different types of photovoltaic devices and technologies throughout the years, so to sort out these technologies, they have been inserted into generations, according to the properties of their materials and evolution of time as well.

The most common solar cells available in the market belong to the first-generation, the single band-gap solar cells, comprised by germanium and the most dominating material in the PV market, silicon. Silicon is one of the most abundant materials on Earth, accounting about 25% of its crust, as well as being very cheap and it's easily producible. [8]

The second-generation is based on thin film technologies. This technology was introduced to reduce the material usage from the previous solar cells, achieving layers as thin as tens of micrometers or even nanometers. This layer is deposited on a layer of substrate such as glass, stainless steel or plastic and due to the thinness of this layer it is possible to build flexible devices that can have many different applications. Some examples of second-generation materials are amorphous silicon, gallium arsenide and copper indium gallium diselenide (CIGS) [9].

There is also the third-generation, which includes the non-based silicon solar cell materials, such as perovskite solar cells (PSC), organic solar cells (OSC) and dye-sensitized solar cells (DSSC). These types of photovoltaic technology use a combination of organic and inorganic materials to generate electron-hole pairs, hence creating a photovoltaic effect throughout several layers. Despite some of these cells still struggle to provide a good efficiency, significant progress on the power conversion efficiency (PCE) of these cells is being made, guaranteeing a promising future for this technology. [1] [11]

IV. SIMULATION

To analyse and perform different simulations on the behaviour of solar cell materials, a 2D PIN solar cell model was considered.

A PIN structure (p-i-n) consists of 3 layers of semiconductors, a p-type layer, an n-type layer and an intrinsic layer (i-layer). By adding this i-layer, it is possible to reduce the surface recombination, which has an influential role on the generated current of a solar cell, especially on small area ones [5]. The i-layer also provides a wider depletion region, increasing the minority carrier diffusion length as well as strengthening the charge carrier lifetime (which reduces recombination).

The 2D model was designed in the *COMSOL Multiphysics* software. To better understand the model at hand, Figure 2 facilitates the comprehension. Breaking down into a more detailed approach of the PIN layers of the generated 2D model. As it was demonstrated before, the PIN module is composed by 3 layers: p-layer, i-layer and n-layer. For this 2D model approach, the same layers were taken into consideration, however as it can be seen in the schematic.

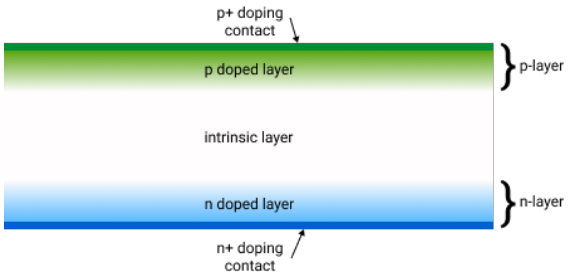

Fig. 2. Illustration of the used solar cell PIN model.

The p-layer and the n-layer are both composed by a heavily doped contact at the top (p+) and bottom (n+) of the cell respectively. In addition, there is also a larger p and n doped areas that contain less dopant (about 100 times less). The role of this second layer is to facilitate the diffusion of the carriers throughout the solar cell, in order to generate the intrinsic layer in between.

Successfully creating the 2D solar cell model, the simulations were ready to start. The main targeted materials in this section is the Silicon and CIGS. In addition, CIGS is also a material that must be treated somewhat differently, for two reasons.

- The CIGS solar cell is comprised of many other layers. And as it was seen before the absorber layer, CIGS, acts as the p-type material of intire cell;
- CIGS has a few properties, such as the band gap and the electron affinity and , that depend on the concentration of gallium.

In this particular case, for the n-layer section of the CIGS PIN model, the donor density used will be equal to the doping of the CdS buffer layer, simulating the interface between CIGS and the buffer.

The gallium dependent values for CIGS offer the possibility to conduct a deeper study of the responsivity and current-power relationship for different concentrations of CIGS.

Previous studies of the CIGS material, from Isabela et. al and P.D. Paulson have used specific values for the concentration of Gallium to compute their results [10] [4]. The results can be observed in Table I.

TABLE I
BAND GAP AND ELECTRON AFFINITY VALUES FOR EACH PERCENTAGE OF GALLIUM IN CIGS, GIVEN BY ISABELLA ET. AL STUDY [4]. TO $x = 0$ THE CIGS SOLAR CELL HAS NO PERCENTAGE OF GALLIUM, THUS HOLDS THE NAME CIS, WHILE THE SAME CAN BE SAID FOR $x = 100$, THE CELL HAS NO INDIUM, THEREFORE CGS.

	x	Band gap (eV)	Electron Affinity (eV)
CIS	0	1.023	4.57
CIGS-31	0.31	1.208	4.25
CIGS-45	0.45	1.351	4.1
CIGS-66	0.66	1.457	3.93
CGS	1	1.771	3.87

1) Responsivity: In this study, the responsivity of the solar cells were extracted. The different solar cell materials were tested with the PIN model, with the primary goal of validating the model, by checking how similar do the responsivity curves match the already known curves of the referred materials.

Firstly the silicon solar cell was the first material to be tested. Silicon has an absorption range of about $740nm$, starting to absorb radiation at the $370nm$, which means for UV radiation, Si solar cells cannot work properly. However, it is possible to see a steadily rise in the materials responsivity, generating higher currents throughout the whole visible spectrum, but for Infra-red radiation, silicon has a huge spike, achieving a maximum of $0.778\mu A/W$ at $1030nm$.

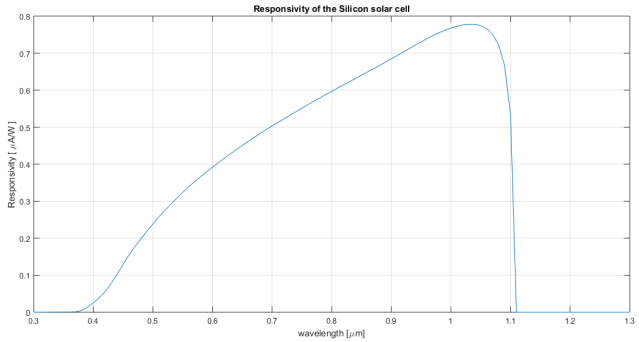

Fig. 3. Responsivity of silicon

For the CIGS responsivity, the concentration of Gallium was taken into consideration, due to the influential role it was when determining certain material properties. After running the simulation for different types of CIGS, it is clearly possible to visualize a decrease of the wavelength for maximum responsivity, as the concentration of gallium increases. This reaction is logical since the increase of gallium within the CIGS cell increases its band gap, thus narrowing its absorption range. The responsivity also decreases when the gallium concentration is increased.

The CIGS solar cell presents itself on the simulation with very low responsivity, when in theory, the results should be relatively close to the silicon solar cell. Since a CIGS cell is composed of more other 3 layers (minimum), each of

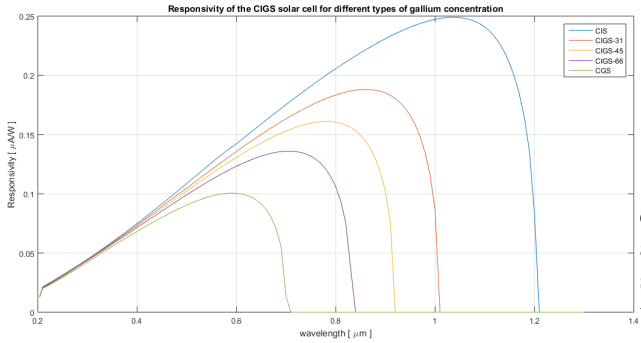

Fig. 4. Responsivity of CIGS

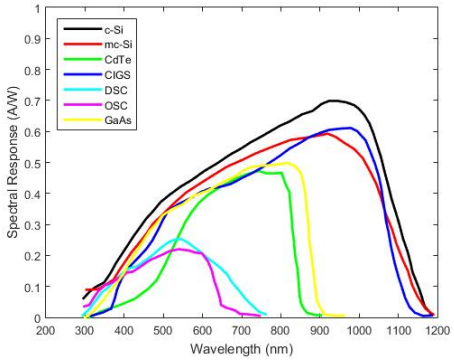

Fig. 5. Responsivity for different solar cell materials, including CIGS and Silicon solar cells. [**?**]

them with their own band gap and doping density, it could explain why the generated current per incident power is so low, as the CIGS absorber layer requires the presence of the other layers in order to unlock its full potential. However, the theoretical results do not reveal the concentration of Ga, but this previous reason can also play a crucial role in widening the absorption band, since the theoretical CIGS has almost the same absorption range as the simulated CIS.

2) Current-Power Relation: The next simulation to be executed is the Current-Power relation. The goal of this simulation is to check the linearity between the generated current of the solar cell, I_L, and the incident radiation power, P_{in}.

To better represent the correlation of current and power, it was used the *polyfit* function from *MATLAB* to find the equation that best fit the data, better described by the equation 11.

$$P(x) = p_n x^n + p_{n-1} x^{n-1} + p_{n-2} x^{n-2} + ... + p_0 \quad (11)$$

To achieve better results of the of the I(P) characteristics, specific wavelengths were taken into consideration, as shown in Table II

Starting with **silicon**, it was possible to verify that for all the studied wavelengths the generated current from the solar cell has a linear relation with the incident light's power. Starting from the UV wavelength, the absorption of the silicon cell is very close to zero, since the responsivity for silicon solar

TABLE II
SELECTED WAVELENGTHS TO STUDY THE I(P) CURVES

Spectrum region	UV	Blue	Green	Orange	IR
Wavelength [nm]	300	420	550	690	800-1100

cells at the UV mark is practically null. As the wavelengths are increased, the slope of each function increases as well, since the responsivity of silicon reaches its peak at $1000nm$, which corresponds to the IR region.

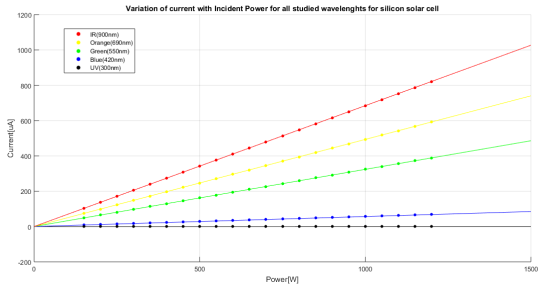

Fig. 6. I(P) curve for Silicon solar cell.

TABLE III
EXTRACTED COEFFICIENTS FROM THE *polyfit* FUNCTION OF THE SILICON SOLAR CELL I(P) DATA POINTS

Wavelength	UV (300nm)	Blue (420nm)	Green (550nm)	Orange (690nm)	IR (900nm)
p_1	1.04E-4	0.057	0.324	0.493	0.685
p_0	5.87E-7	-3.09E-5	-0.001	-0.003	-0.006

Once again, for **CIGS** the Ga concentration was considered. Since it is a more complex material than silicon, some differences are expected in the I(P) characteristics.

CGS holds the smallest responsivity window, so in the IR region, there is no absorption. For the smallest wavelengths, around the UV mark, the CGS material presented to have a linear increase in current with the increase of power. On the other hand, once the wavelength starts increasing, the I(P) function starts to drift away from its linear shape, assuming a slightly curved shape. This small curved shape starts getting a bit more noticeable as the wavelength increases. Along with the curving, the slope begins to increase as well, which is a natural response of the material's responsivity.

Nevertheless, once the wavelength for maximum peak of current is surpassed (590nm), the produced current is decreased. This is why the green radiation can produce higher output currents, Figure 7.

For **CIGS-66** and **CIGS-45**, the orange light still is the highest generated current of the remaining wavelengths under study, although the IR radiation for the CIGS-45 has a higher absorption, meaning it will not pass through the solar cell nor reflect.

At **CIGS-31** it is possible to verify that the IR radiation has surpassed the orange radiation when it comes to the generated

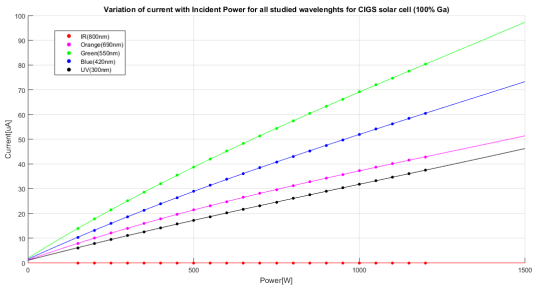

Fig. 7. I(P) curve for the CGS solar cell.

TABLE IV
COEFFICIENTS OF THE 3RD ORDER POLYNOMIAL EXPRESSION THAT BEST FITTED CGS, FOR THE DIFFERENT WAVELEGTHS.

Wavelength	UV (300nm)	Blue (420nm)	Green (550nm)	Orange (690nm)	IR (900nm)
p_3	1.906E-9	3.598E-9	5.69E-9	-3.588E-9	-
p_2	-5.998E-6	-1.409E-5	-2.132E-5	-1.411E-5	-
p_1	0.0348	0.0609	0.083	0.047	-
p_0	1.045	1.529	1.973	1.20	-

current, achieving a maximum of $143.7\mu m$. Nonetheless, no changes were found on the curvature of the I(P) function for each specific wavelength from the previous Figure.

With the **CIS** solar cell, the responsivity range reaches its maximum, thus the maximum current peak surpassed the maximum wavelength at study, so it was required to increase the study range for the IR region, so the $1100nm$ mark was added. This increase in the IR region, could prove that as the wavelength rises the non-linearity of CIGS increases further, since it is possible to get almost the same maximum current for both of $900nm$ and $1100nm$ wavelengths.

On a general conclusion, after observing every I(P) function of the solar cell, it is safe to assume a possible relationship of the non-linearity to the increase of wavelength, since most of the non-linear results occur above the green radiation. This non-linearity can also be spotted in a more early stage, more specifically in the blue radiation for CGS, because the absorption range is very small.

V. EXPERIMENTAL RESULTS

For this study, the efficiencies, fill factors and characteristic curves are the electrical properties of the PV panels that were evaluated. It was planned to test one type of solar cell material that represented each of the three generations of PV technology. **Crystalline silicon** (c-Si) was chosen to represent the 1st generation, **CIGS** the 2nd generation and **DSSC** the 3rd generation. The studies conducted to the crystalline silicon and the CIGS solar cell materials provided the required information to produce the necessary results. However, the results obtained from the DSSC study were mainly inconclusive, since the DSSC cell had no contacts to connect the necessary equipment and measure the output voltage of the cell. Due to the small area of the DSSC ($2.04cm^2$) it was also expected to produce a very small output voltage and current, uncertain

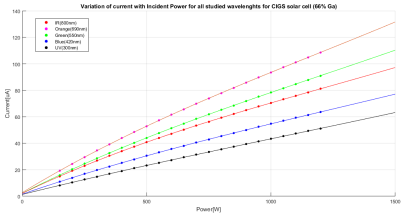

Fig. 8. I(P) curve for the CIGS-66 solar cell.

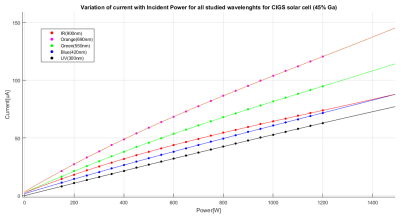

Fig. 9. I(P) curve for the CIGS-45 solar cell.

Fig. 10. I(P) characteristics for CIGS-66 and CIGS-45.

TABLE V
COEFFICIENTS OF THE 3RD ORDER POLYNOMIAL EXPRESSION THAT BEST FITTED CIGS-66, FOR THE DIFFERENT WAVELEGTHS.

Wavelength	UV (300nm)	Blue (420nm)	Green (550nm)	Orange (690nm)	IR (800nm)
p_3	2.063E-9	4.094E-9	7.16E-9	9.251E-9	8.038E-9
p_2	-6.639E-6	-1.569E-5	-2.595E-5	-3.283E-5	-2.991E-5
p_1	0.047	0.065	0.095	0.1143	0.090
p_0	1.311	1.56	2.259	2.790	2.177

that the multimeter would be able to measure these signals, since it could have fallen off the range of the device.

A. I(V) curves and efficiencies

The two solar cells were tested under the same conditions with the same equipment under total illumination of the projector, at $115W/m^2$. However, in order to compare both electrical properties of these solar cells, the effective area must be taken into consideration, since both cells have very distinctive sizes. Since it was not possible to determine directly the I_{SC} for the CIGS PV panel, a linear regression was made to better determine the exact value of I_{SC} per effective area.

It is possible to verify that the I(V) curve for silicon is very close to the ideal model of a solar cell. The deviations from the ideal model comes from the possible shunt resistance, R_{sh} or series resistance, R_s that are generated by small imperfections of the layers or conduction losses of the connecting wires.

Taking a more closer look at the CIGS I(V) characteristic, the following conclusions were withdrawn:

- **For** $5.16V$ **and** $5V$ the CIGS panel's current rapidly increases at huge slope, as it should be, comparing to the ideal model. The curve of the cell is a bit more abrupt than the ideal model, but it could be caused by the heterojunction of different materials. This alludes to a possible internal low series resistance within the model, because the series resistance dictates the slope of this

TABLE VI
COEFFICIENTS OF THE 3RD ORDER POLYNOMIAL EXPRESSION THAT BEST FITTED CIGS-45, FOR THE DIFFERENT WAVELEGTHS.

Wavelength	UV (300nm)	Blue (420nm)	Green (550nm)	Orange (690nm)	IR (900nm)
p_3	-7.805E-10	2.44E-9	7.728E-9	-1.077E-8	9.008E-9
p_2	-3.24E-7	-8.153E-6	-2.766E-5	-3.744E-5	-3.187E-5
p_1	0.0539	0.0649	0.0991	0.127	0.085
p_0	-0.0253	1.632	2.382	3.268	2.433

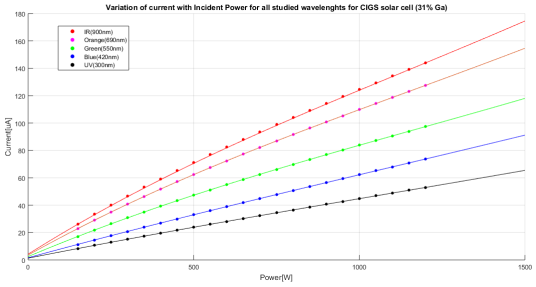

Fig. 11. I(P) curve for the CIGS-31 solar cell.

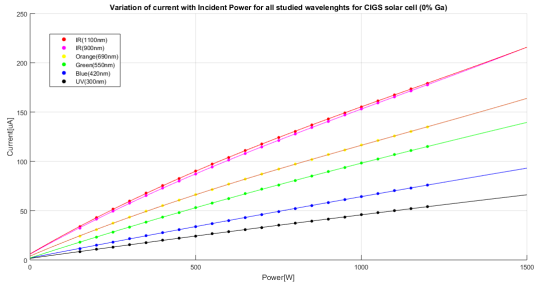

Fig. 12. I(P) curve for the CIS solar cell.

TABLE VII
COEFFICIENTS OF THE 3RD ORDER POLYNOMIAL EXPRESSION THAT BEST FITTED CIGS-31, FOR THE DIFFERENT WAVELENGTHS.

Wavelength	UV (300nm)	Blue (420nm)	Green (550nm)	Orange (690nm)	IR (900nm)
p_3	1.997E-9	2.456E-9	8.13E-9	1.169E-8	1.363E-8
p_2	-6.446E-6	-7.988E-6	-2.888E-5	-4.023E-5	-4.770E-5
p_1	0.048	0.066	0.102	0.135	0.154
p_0	1.284	1.622	2.468	3.557	4.245

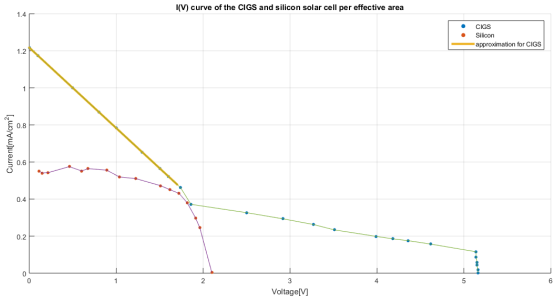

Fig. 13. I(V) curve for Silicon and CIGS per effective area.

region. The higher the slope, the less influence will the series resistance, R_s, have on the circuit;

- **From** $5V$ **to** $2V$ the current is steadily increasing, contradicting the very slow increase and stabilization of the current at the I_{SC}. Nevertheless this behaviour is not totally unrecognizable. When the shunt resistances of a solar cell are very low, there is an increase of the slope for this region, thereby enforcing the possibility of an internal shunt resistance within the CIGS solar cells.
- **From** $2V$ **to** $1.6V$ the slope increases drastically. At this point the resistance of the load is at its minimum value (10Ω). The only plausible explanation to this dramatic shift is given by M. Burgelman study on CIGS material. On his study, he proved the existence of inlayer resistances that were formed during the fabrication process which could behave as shunt resistances. This resistance is formed naturally during fabrication, however since the CIGS solar panel under analysis is flexible, the fabrication process must have been different from regular rigid thin-film solar cells. Therefore, the shunt resistance effect was amplified. [7]
- **From** $1.6V$ **to** $0V$ there are no values shown, however with the previous conclusions, it is safe to assume that the linear behaviour would remain identical and to better represent these results a linear regression was considered to determine the value of the I_{SC} of the CIGS panel.

It is possible to verify that the the highest V_{OC} and I_{SC} per area are registered on the CIGS solar panel. A possible explanation for this result could be the number of solar cells within the panel and how they are connected: in series or in parallel.

The crystalline Silicon solar panel registered a 6.43% efficiency with a fill factor of 64.03%. Despite the low efficiency, the obtained fill factor is very high, which is good. Moreover, the CIGS flexible panel achieved a a higher efficiency than Silicon, but its fill factor is drastically low, since the "squareness" of the CIGS I(V) curve is far from the ideal one.

1) Light absorption: In this section, the responsivity for each panel was compared with the emission spectrum of the projector light. It was used the simulation results in order to achieve this comparison. This connection of parameters, can allude to the better understanding of the performance of the solar panels.

The lighting projector used in the experiment is the Ersetze Jede Gebrochene Schutzscheibe R7s 500W max, composed of an halogen light bulb type. Since the only solar cells that

TABLE VIII
COEFFICIENTS OF THE 3RD ORDER POLYNOMIAL EXPRESSION THAT BEST FITTED CIS, FOR THE DIFFERENT WAVELENGTHS.

Wavelength	UV (300nm)	Blue (420nm)	Green (550nm)	Orange (690nm)	IR (900nm)	IR (1100nm)
p_3	1.943E-9	2.414E-9	2.7E-9	1.270E-8	1.722E-8	1.838E-8
p_2	-6.279E-6	-7.846E-6	-1.571E-5	-4.32E-5	-5.749E-5	-6.475E-5
p_1	0.049	0.068	0.109	0.143	0.1875	0.196
p_0	1.255	1.593	2.042	3.987	5.869	6.173

TABLE IX
EXTRACTED ELECTRICAL PROPERTIES OF THE SILICON AND CIGS SOLAR PANELS.

	$V_{OC}(V)$	$I_{SC}(mA/cm^2)$	$I_{max}(mA/cm^2)$	$V_{max}(V)$	$P_{max}(mW/cm^2)$
Silicon	2.10	0.552	0.4308	1.723	0.7422
CIGS	5.16	1.217	0.2625	3.27	0.8584

TABLE X
FILL FACTOR

	FF (%)	η (%)
Silicon	64.03	6.43
CIGS	13.67	7.44

were used in this experiment were the CIGS and crystalline silicon ones, only the absorption's of these two materials will be considered [12]. In case of CIGS, three of the five CIGS types used in this study were considered: CIS, CGS and CIGS-45. These three compounds were selected in order to represent the three possible corner cases of gallium concentration in CIGS.

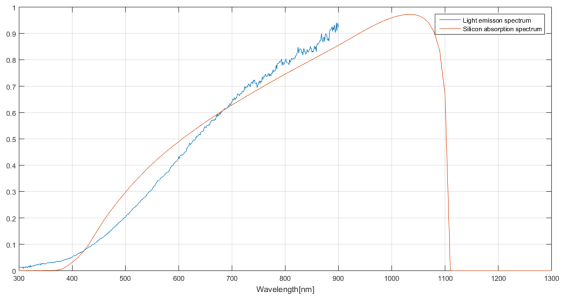

Fig. 14. Emission spectrum for the halogen light projector.

Silicon's efficiency presented to be lower than the CIGS panel, but nonetheless its FF proved that the main problem was related to the area of the cell. When the responsivity is crossed with the emission spectrum of the light projector, it is possible to check the following:

- **Between the** $300nm$ **and** $380nm$ silicon does not absorb any of the incident light, since this corresponds to the UV region. Even if it was inside the absorption spectrum of silicon, the amount of irradiated light would be very little, absorbing in both cases no UV radiation whatsoever.
- **For the** $400nm$ **and the** $700nm$ silicon's responsivity starts increasing at a fast pace, even surpassing the light projector's irradiation. The light emission also increases, but not as steep as the silicon's responsivity at first. Nonetheless, radiation absorbed will be absorbed by the solar cell, since both functions are increasing and also because silicon has a very high current generation at this gap.
- **From** $700nm$ **to** $900nm$ the light emission reaches its peak. Despite the silicon's responsivity peak at $1040nm$, the responsivity still circles the 70% all the way up to 90% around the red and IR region.

This shows how high the current can be generated in the silicon material for this particular light. However, the experimental results don't share the same statement, because the CIGS I_{SC} per area is higher than Silicon's.

Moving on to CIGS, it is possible to verify that the absorption range of each cell is reduced as the Gallium concentration increases.

- **At the** $200nm$ **to** $400nm$ region of the graph, it is possible to verify that little to zero radiation will be generated into current, due to the lack of light emission at that region, regardless of the concentration of gallium.
- **From the** $450nm$ **to** $900nm$ the light emission starts increasing and so does the CIGS responsivity. At this mark, the gallium concentration comes into action. Analysing for CGS first, the cell starts producing current at $710nm$, this means that only the visible spectrum will be absorbed by the cell and transformed into current. This means that the generation of current from the light will be very small, since most of its highest wavelengths will pass through the cell or will be reflected, as the wavelengths that are encompassed in the responsivity of CGS, will produce current equivalent to 40% of CIS maximum. For the CIS solar cell the highest peak in responsivity is located on $1060nm$, which implies that no light will reach the maximum current generation point. However, on this window, the maximum emission of the light projector is very close to the maximum of absorption, which means that more current will be produced. The generated current will be high, but not as high as if it compared to silicon, since it's much lower. The CIGS-45 cell is the middle ground between the CGS and the CIS, since its responsivity peak is around 780nm about 60% of the CIS maximum and stops absorbing at $920nm$.

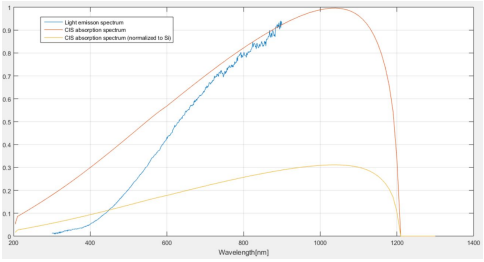

Fig. 15. Comparison of the light emission spectrum with CIS responsivity.

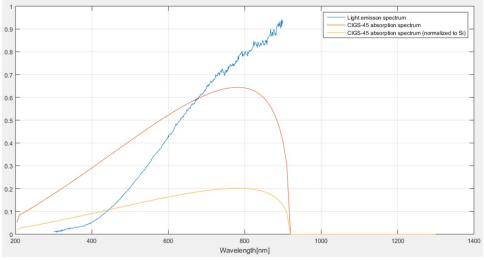

Fig. 16. Comparison of the light emission spectrum with CIGS45 responsivity.

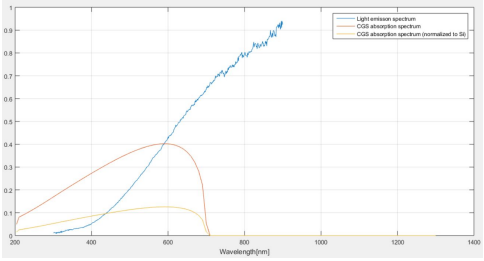

Fig. 17. Comparison of the light emission spectrum with CGS responsivity.

Fig. 18. The three different responsivities of CIGS, for different percentages of gallium.

This material can absorb throughout the whole emission spectrum of light, making it a good candidate for the assumption of the type of CIGS material.

Through this analysis it is possible to assume that the panel used in the experiments does not contain a very large concentration of Ga, since its absorption range is very short and does not match with the experimental results. To solidify this statement, Isabela has proven that CIS can absorb 60% more IR radiation than the CGS solar cells [].

2) V_{OC} analysis: T. Kirchartz and U. Rau in their study have investigated different models that use internal parameters of the solar cell (e.g. mobility carriers, band gap, absorption coefficients) that can be used to obtain performance metrics of solar cells like the V_{OC} [6], using the following equations:

$$V_{OC} = 2kT \cdot \ln\left(\frac{J_{SC}}{qd\frac{\sqrt{N_C N_V}}{2\tau}\exp\left(\frac{-E_g}{2kT}\right)} + 1\right) \qquad (12)$$

In order to use this formula, some assumptions had to be made:

- **Assumption 1** - For starters, to use this equation, it was assumed that the absorber layer of the solar cell was fully depleted.
- **Assumption 2** - Secondly, the internal values of the materials that were used are originated from the simulations.
- **Assumption 3** - Lastly, it was used the obtained I_{SC} per effective area from the experimental results to replace the necessary short circuit current density. As said previously, this assumption implies that the solar panels are composed of only one single solar cell, with the same area as the whole panel.

The experimental values of the V_{OC} are about $5.16V$ and $2.10V$ for the CIGS and silicon solar panel respectively, while the highest theoretical value for V_{OC} is $1.252V$ and $0.704V$ for the CIGS and silicon solar panels respectively.

This means, it is not possible for the the solar panel to represented by just one solar cell and there must be a series of n solar cells, in order to produce the experimental values for V_{OC}, which is why assumption number 3 erroneous and didn't entirely represent the actual reality, thus not been taken into consideration in the previous sections of the experiments.

it is possible to approximately determine the obtained V_{OC} comparing it with the experimental values. For silicon it's possible to see that 3 solar cells generate the same voltage as the entire panel.

For CIGS it is possible to check that the number of required cells decreases every time the gallium concentration is increased, since the voltage gets higher. However, if the solar cells were all in series it is possible to assume that the concentration of the CIGS is panel would be mainly indium, but it is a statement that cannot be entirely certified.

VI. SEM ANALYSIS

SEM stands for Scanning Electron Microscope. This type of microscope is used for observations of surfaces at great detail, using electrons instead of light to form an image from a sample.

This specimen (or sample) when irradiated with a fine electron beam, secondary electrons are emitted from the specimen's surface, hence forming a 2D image as if it was seen from the naked eye.

To better comprehend and to learn about the composition of the studied solar cells, a SEM analysis was conducted. This type of study allows the better understanding of the solar cells at hand.

Starting with the CIGS solar cell, has it can be seen in Figure 19, the SEM image is not fully clear on how many layers there are, but it is clearly possible to see the top encapsulating layer that appears to have a fabric-like texture, as it can be seen by the amount of fibers.

The next material to be analyzed was the silicon solar cell and on this SEM image it was possible to detect clearly different layers, depicted on Figure 20. At the top, there is the possible TCO (transparent conductive oxide) of the solar cell. Although there is no certainty on the type of material that composes this layer, but it safe to say that is an oxide of

TABLE XI
NEW ESTIMATED VALUES OF V_{OC} FOR DIFFERENT NUMBERS OF SOLAR CELLS CONNECTED IN SERIES

Materials	**Silicon**	**CIS**	**CIGS-31**	**CIGS-45**	**CIGS-66**	**CGS**
V_{OC}	0.704	0.512	0.712	0.832	0.972	1.252
Estimated # of cells	3	10	7	6	5	4
Estimated V_{OC}	2.112	5.12	4.984	4.992	4.86	5.008
Experimental V_{OC}	2.12	5.16				

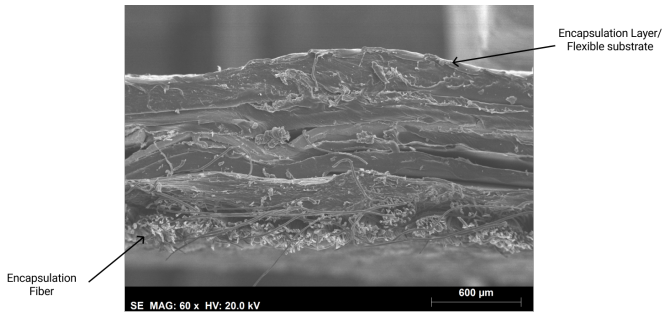

Fig. 19. Cross-sectional SEM image from the CIGS material, with some suggestions of the definition of each layer. Note that the solar panel is upsidedown.

some sort, due to the high presence of oxygen atoms in the top layer.

After the TCO, there is a $225\mu m$ crystalline silicon layer. It's not possible to determine whether it is a P-N or PIN type silicon, because there is no information on the doping of each layer.

The rest of the layers follow the same order. There is a possible Metal/TCO contact with $37.5\mu m$ thickness, followed by a $65.5\mu m$ dieletric coating layer, all built on top of the substrate that can be made from ceramic tile. However, the EDS analysis would come a long way in supporting these assumptions.

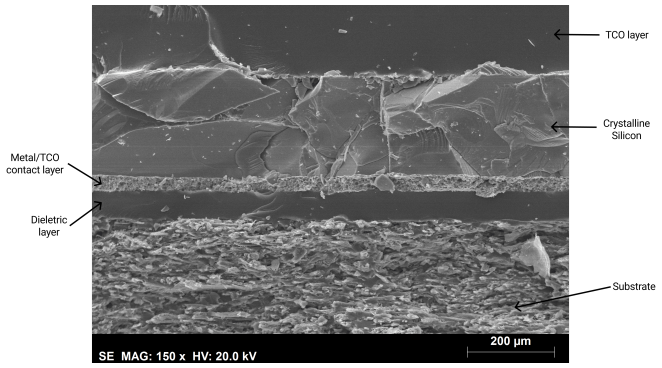

Fig. 20. Cross-sectional SEM image from the silicon cell. It is possible to tell apart each layer of the cell as presented on the image.

Finally the last material to be submitted into the SEM analysis was the DSSC. It is possible to detect a small layer that could correspond to the electrode of the solar cell, as seen in Figure 21. In some types of DSSC it is possible to find some graphene "flakes" deposited on top of the electrode, to better enhance the efficiency of the cell. Above the graphene it is possible to find a compact layer of TiO_2, and it is also possible to assume the irregular spheres throughout the top of the electrode may be porous TiO_2 connected to the dye. However, to be certain of these claims, the EDS analysis had to be taken into consideration.

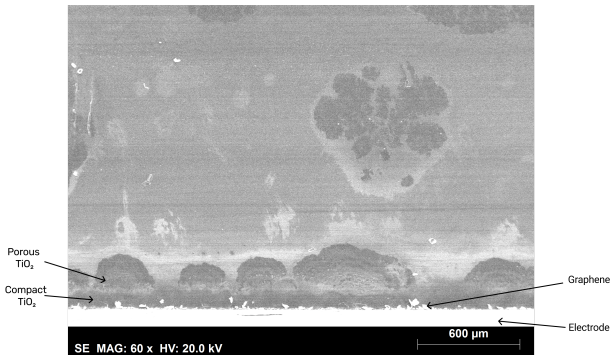

Fig. 21. Cross-sectional SEM image from the DSSC, with some suggestions of the definition of each layer.

VII. CONCLUSIONS AND FUTURE WORK

A. Conclusions

The main goal of this study was to compare some of the most common solar cells from different solar cell generations, like CIGS and silicon and compare some of their properties and parameters.

The 2D PIN model after being validated proved that there is somewhat of a difference when assuming a CIGS solar cell as a PIN structure, although the shape and the absorption range of the CIGS solar cell are very similar to other studied solar cells of the same material. The main difference is located on the amount of generated current. Regardless, the obtained simulated results verify the statement that CIGS can absorb to some extent some UV radiation and IR radiation, just depends on the amount of Indium that is deposited in the fabrication of the cell.

For the silicon solar cell, it was possible to see that the responsivity results were close to what they were expected as well. Being a more simple solar cell, it makes it more easy to recreate it in software.

The relationship between the generated current and power proved that different materials will affect this characteristic. This analysis had the goal of capturing changes in the linear behaviour between incident power and the generated current, so to better understand this, the *polyfit* function in *MATLAB* was used, in order to extract the polynomial expression that

best fitted the data. Silicon proved that first generation materials (homojunctions) have a linear relationship with between current and power, but for CIGS (an heterojunction) proved that the equation that best fitted the output data was a 3rd degree polynomial expression. However, this non-linearity only proved to be true for regions other than the UV, where it remained linear, regardless the concentration of Ga.

Afterwards, the focus was shifted to the real-life scenario, with real solar panels. The CIGS solar cell, proved to have a very high I_{SC}, since for the lowest value of load resistance, the voltage was not close to zero, proving the high illumination current that could be generated from the solar panel. The efficiency was relatevily low for a CIGS panel, but it since this panel was made from a flexible substrate, naturally will achieve lower efficiencies than a rigid CIGS panel.

It was also possible to notice the high impacts that gallium has on this type of material, since fewer concentrations of Ga will increase the short-circuit current, but will cripple the open circuit voltage. So depending on the desired application, CIGS can be molded to fit those needs.

This type of versatility is almost impossible in a traditional silicon solar panel, since there is no way of configuring beforehand how to refine the I_{SC} or V_{OC} of the panel.

Unfortunately, it was not possible to retrive conclusions from the DSSC, although this material is very different than the other generations, it was the first of its generation to flourish and proved that hybrid solar cells could be created and achieve interesting efficiencies.

B. Future Work

For future studies and research in this topic, there is always room for improvement. The model that was created was mainly built from a semiconductor point of view, where it was possible to define the doping and the electrical properties of the material, but thanks to inclusion of the Multiphysics option of *COMSOL*, it was possible to generate a controlable incident radiation, where power and frequency could be user-defined.

The main upgrade that should be taken into consideration in future studies, is the design of a more realistic solar cell, given each cell is comprised of other elements that in real-life scenarios may affect its behaviour, such as the encapsulation materials and the other layers (in case of CIGS) that constitute the cell at hand.

Of course the upgrade from a 2D model to a 3D model will bring much close to reality results, since it is truly possible to recreate a solar cell in a laboratorial environment. However, new photovoltaic technologies should also include a study of the solar cell, under direct sunlight and outdoor exposure, since it can draw the physical limitations of these solar cells as well as the affect of environmental conditions on the devices under study.

Some of these new PV technologies are targeting the market of small applications, so that it will work as complementary energy system, many of it in the forms of flexible solar cells. This emerging technology, could also be submitted under stress bending tests in order to determine its limitations and affect to voltage and current produced.

REFERENCES

[1] Bulent G. Akinoglu, Bilge Tuncel, and Viorel Badescu. Beyond 3rd generation solar cells and the full spectrum project. recent advances and new emerging solar cells. *Sustainable Energy Technologies and Assessments*, 46:101287, 2021.

[2] António Batista, Carlos F. Fernandes, Jorge Pereira, and José Paisana. Capítulo 1 - semicondutores. In LIDEL, editor, *Fundamentos da Eletrónica*, pages 1 – 91. 2012.

[3] Corsin Battaglia, Andres Cuevas, and Stefaan De Wolf. High-efficiency crystalline silicon solar cells: status and perspectives. *Energy Environ. Sci.*, 9:1552–1576, 2016.

[4] Isabela C. B., Ricardo A. Marques Lameirinhas, João Paulo N. Torres, and Carlos A. F. Fernandes. Comparative study of the copper indium gallium selenide (cigs) solar cell with other solar technologies. *Sustainable Energy Fuels*, 5:2273–2283, 2021.

[5] Ali Imran, Jianliang Jiang, Deborah Eric, Muhammad Zahid, and Muhammad Yousaf. Parametric optimization of gaas pin solar cell. 08 2018.

[6] Thomas Kirchartz and Uwe Rau. What makes a good solar cell? *Advanced Energy Materials*, 8(28):1703385, Oct 2018.

[7] A.Niemegeers M.Burgelman. Calculation of cis and cdte module efficiencies. https://users.elis.ugent.be/ELISgroups/solar/projects/scaps/MDS/Burgelman

[8] Preeti Nain and Arun Kumar. Theoretical evaluation of metal release potential of emerging third generation solar photovoltaics. *Solar Energy Materials and Solar Cells*, 227:111120, 2021.

[9] Sukanchan Palit and Chaudhery Mustansar Hussain. Chapter 1 - engineered nanomaterial for industrial use. In Chaudhery Mustansar Hussain, editor, *Handbook of Nanomaterials for Industrial Applications*, Micro and Nano Technologies, pages 3–12. Elsevier, 2018.

[10] P. D. Paulson, R. W. Birkmire, and W. N. Shafarman. Optical characterization of cuin1xgaxse2 alloy thin films by spectroscopic ellipsometry. *Journal of Applied Physics*, 94(2):879–888, 2003.

[11] Tetsuo Soga. Chapter 1 - fundamentals of solar cell. In Tetsuo Soga, editor, *Nanostructured Materials for Solar Energy Conversion*, pages 3 – 43. Elsevier, Amsterdam, 2006.

[12] Unknown. Lamp spectra. https://guaix.fis.ucm.es/lamps$_spectra.[Online; accessed16$ $September - 2021]$.